IJAME

Int. J. of Applied Mechanics and Engineering, 2026, vol.31, No.4, pp.162-180
DOI: 10.59441/ijame/224472

INTEGRATED RELIABILITY-BASED DESIGN OPTIMIZATION FRAMEWORK FOR COST-RISK ANALYSIS OF SFRC DEEP BEAMS: LOAD SENSITIVITY AND CONFIGURATION COMPARATIVE STUDY

P. Tran and A. Hoang*
[1]Faculty of Civil Engineering, University of Architecture Ho Chi Minh City, VIET NAM
E-mail: an.hoangbac@uah.edu.vn

This paper proposes an integrated Digital Reliability-Based Design Optimization (RBDO) Framework for Steel Fiber Reinforced Concrete (SFRC) deep beams, aiming to minimize Life-Cycle Cost (LCC) while ensuring structural safety under stochastic uncertainties. Addressing the computational inefficiency of traditional Monte Carlo simulations (MCS) in optimization loops, the study introduces a High-Fidelity Discrete Surrogate Model. This model utilizes a pre-computed lookup database derived from a full factorial discretization of the design space ($(N = 2{,}541$ points$)$, allowing for $O(1)$ complexity retrieval and eliminating interpolation errors near limit state boundaries. The underlying mechanical model is based on a modified Strut-and-Tie Model (STM), rigorously validated against an extended experimental database of 48 specimens (including independent datasets). Statistical analysis confirms the model's robustness, achieving an unbiased Mean Experimental-to-Predicted ratio $\left(V_{exp} / V_{pred}\right)$ of 0.97 and a low Mean Absolute Error (MAE), despite the inherent scatter in shear behavior $(R^2 = 0.43)$. By integrating the Non-dominated Sorting Genetic Algorithm II (NSGA-II) with the Discrete Surrogate Model, the framework achieves a computational speed-up of approximately 8×10^4 times compared to direct MCS. The optimization results reveal a critical economic "tipping point" at a load intensity of $600\ kN$, beyond which SFRC solutions demonstrate superior cost-efficiency over conventional stirrup reinforcement. The proposed digital workflow provides structural engineers with a rapid, physically grounded, and statistically verified tool for the sustainable design of critical transfer members in high-rise buildings.

Keywords: deep beams, Steel Fiber Reinforced Concrete (SFRC), Reliability-Based Design Optimization (RBDO), discrete surrogate model, Life-Cycle Cost (LCC)

1. Introduction

The paradigm of structural engineering is undergoing a significant transformation, driven by the rise of powerful computational tools and "Digital Technology Driven Engineering". The industry is progressively moving from traditional, deterministic design philosophies towards sophisticated, simulation-driven, performance-based approaches. In the context of advanced structural mechanics, structural optimization plays a pivotal role in enhancing both engineering efficiency and mechanical performance. By optimizing material usage and enhancing structural reliability through advanced composites like Steel Fiber Reinforced Concrete (*SFRC*), engineers can extend the service life of critical infrastructure, thereby minimizing the total cost of ownership associated with maintenance or premature failure [1, 2]. However, the shear behavior of SFRC deep beams is intricate, characterized by a complex stress transfer mechanism that depends heavily on the interaction between concrete struts, steel ties, and fibers [3, 4].

Recent studies have extensively investigated the shear behavior and modeling of deep beams. For instance, Megahed [5] performed a comprehensive reliability analysis of shear strength models for deep beams, highlighting the superior performance of data-driven approaches over traditional code-based formulations.

* To whom correspondence should be addressed.

Meanwhile, recent efforts by Rahimi *et al.* [6] and Kavya *et al.* [7] have successfully applied optimization strategies and hybrid machine learning models to enhance the structural performance and shear strength prediction of reinforced concrete members. These studies demonstrate the growing potential of digital tools in solving complex structural problems.

However, significant gaps remain in the existing literature. First, most optimization studies rely on deterministic approaches, neglecting the stochastic nature of loads and material properties which are critical for deep beams prone to brittle shear failure. Second, while the mechanical behavior of SFRC is well-documented, a comprehensive Life-Cycle Cost (LCC) analysis that quantifies the economic justification of fibers under varying load intensities is missing. Third, previous works predominantly focus on simply supported configurations, leaving the reliability performance of continuous SFRC deep beams – which exhibit complex shear redistribution – largely unexplored.

To address these gaps, this study proposes an integrated Digital RBDO Framework. The distinct contributions of this paper are:

I. Methodological innovation: the development of a High-Fidelity Discrete Surrogate Model based on a pre-computed database of $2{,}541$ design points. This approach allows for $O(1)$ complexity retrieval, achieving a computational speed-up of approximately 8×10^4 times compared to direct simulations while eliminating interpolation errors.

II. Robust validation: unlike previous studies that rely on limited data, the mechanical model in this study is rigorously validated against an extended database of 48 specimens, including independent datasets from literature. The model achieves an unbiased Mean Experimental-to-Predicted ratio of 0.97, ensuring statistical robustness.

III. Strategic insight: the identification of a specific economic "tipping point" $(600\ kN)$ and the comparative analysis between simply supported and continuous configurations, providing a quantitative guideline for the cost-effective application of SFRC in high-rise building transfer structures.

2. Reliability-Based Design Optimization framework

The proposed framework is a computational methodology for solving Reliability-Based Design Optimization (RBDO) problems [8-10]. Its architecture, as illustrated in Fig.1, is implemented in three distinct phases:

Phase 1: Pre-Processing and Surrogate Modeling: A "Direct Sampling Lookup Table" is constructed using High-Fidelity Monte Carlo Simulation (10^7 samples) to map the discrete design space to failure probabilities (P_f).

Phase 2: Multi-Scenario Optimization Loop: The NSGA-II algorithm executes the optimization. Uniquely, this process is wrapped within a "Load Sensitivity Loop" covering five load scenarios $(P_{baseline} = 500 \text{ to } 700\ kN)$.

Phase 3: Post-Processing and Decision Making: A Life-Cycle Cost (LCC) analysis is performed to identify the optimal design strategy and the economic "tipping point."

The specific components of this framework are detailed in the following subsections.

2.1. Optimization engine: NSGA-II

The core of the frameworks is the Non-dominated Sorting Genetic Algorithm II (NSGA-II), a powerful evolutionary algorithm developed by Deb *et al.* [11]. This algorithm is selected for its proven efficiency in exploring complex, non-convex search spaces and its ability to find a well-distributed set of diverse solutions [12]. It operates on a population of designs, iteratively applying genetic operators (selection, crossover, and mutation) to converge towards the true Pareto-optimal front. A Pareto front represents a set of non-dominated solutions, where no single objective (e.g., cost) can be improved without degrading the other objective (e.g., safety).

To ensure strict adherence to the discrete design space defined by the Lookup Table (Phase 1), the algorithm utilizes an integer-based encoding scheme. The genetic operators (crossover and mutation) manipulate the indices of the design variables within the pre-defined arrays (e.g., selecting the index corresponding to $h = 500\ mm$) rather than modifying the continuous values. This mechanism guarantees that every generated offspring corresponds exactly to a valid, constructible design point. Regarding the convergence criterion (as shown in Fig.1, a fixed maximum number of generations (10) was used as the stopping criterion. Preliminary trials indicated that the population stabilizes along the Pareto front within this range due to the constrained and discrete nature of the design space.

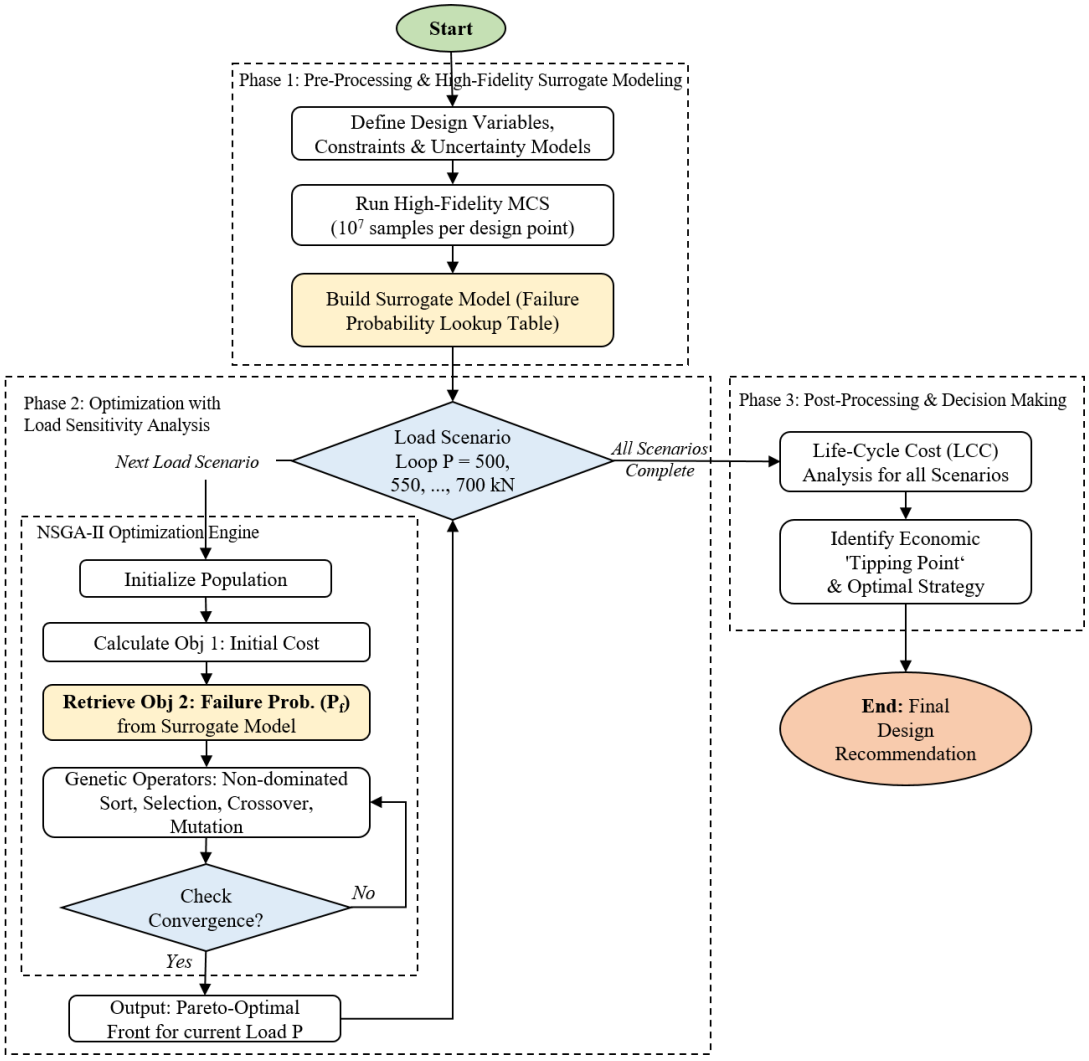


Fig.1. Flowchart of the proposed Digital Framework incorporating High-Fidelity Surrogate Modeling and Load Sensitivity Analysis.

2.2. Objective function 1: Initial cost $(C_{Initial})$.

The first objective function quantifies the initial construction cost. It is a deterministic function of the design variables (beam geometry, reinforcement ratios, fiber content). The goal is to minimize this function, which is calculated as the sum of the costs of concrete, reinforcing steel (longitudinal and transverse), and steel fibers [13, 14].

$$C_{Initial} = C_{concrete} + C_{rebar} + C_{fiber} + C_{formork},$$
$$C_{Initial} = V_{conc}.G_{conc} + M_{rebar}.G_{rebar} + M_{fiber}.G_{fiber} + A_{formwork}.G_{formwork}, \quad (2.1)$$

where: V is the volume of concrete, M is the mass of steel and fiber, A is the area of formwork, and G is the unit price for each material. For the calculation of initial costs, the following unit prices were adopted based on current market rates in the study region: concrete $\left(G_{conc} = 75USD/m^3\right)$, reinforcement steel $\left(G_{rebar} = 0.74\ USD/kg\right)$, steel fibers $\left(G_{fiber} = 1.80\ USD/kg\right)$, and formwork $\left(G_{formwork} = 20USD/m^2\right)$.

2.3. Reliability analysis using surrogate modeling

Limit State Definition: The limit state function $g(X)$ [15] is defined based on the Ultimate Limit State (*ULS*) for shear failure, which is the governing failure mode for deep beams. The failure condition is mathematically expressed as:

$$g(\boldsymbol{X}) = V_u(\boldsymbol{X}) - V_{load}, \quad (2.2)$$

where:

- $V_u(X)$: The random shear resistance predicted by the proposed Surrogate Model. This is calculated using a modified Strut-and-Tie Model (*STM*) that accounts for both stirrups and steel fibers [16-18]. The model for R is based on a modified STM validated against a comprehensive experimental program [3, 4, 19].
- $V_{load} = P_{factor}(D + L)$: The random shear demand, derived from dead (D) and live (L) loads.
- X (Random Variables): Key parameters are treated as random variables, not fixed values. This includes load components $(D,\ L)$, material properties (concrete strength, steel yield strength), and model uncertainties, with their statistical distributions (mean, *COV*, distribution type) adopted from established sources like the JCSS Probabilistic Model Code (Tab.1) [20].

Target reliability: in accordance with the JCSS Probabilistic Model Code [20] and EN 1990, the target reliability index is set to $\beta_{target} = 3.8$ for a *50*-year reference period (Reliability Class *RC2*, moderate consequences of failure). This value serves as the constraint boundary for the optimization algorithm.

The probability of failure $\left(P_f\right)$ [8] can be estimated using the Monte Carlo Simulation method as follows:

$$P_f \approx \frac{1}{N}\sum_{i=1}^{N} I(g_i < 0), \quad (2.3)$$

where N is the number of simulations, and $I(\bullet)$ is the indicator function which equals *1* if $g_i < 0$ (failure) and *0* otherwise.

Theoretically, the probability of failure is estimated using Eq.(2.3). However, performing a direct Monte Carlo Simulation (MCS) with high precision $\left(N = 10^7\right)$ for every candidate solution within the NSGA-II optimization loop is computationally prohibitive.

To address this computational challenge, this study employs a high-fidelity Discrete Surrogate Model instead of online simulations. The construction of the surrogate database involved a full factorial discretization of the design space based on practical constructability constraints:

- Concrete strength $\left(f_c^{'}\right)$: Discretized in $5\ MPa$ intervals (from 30 to $80\ MPa$).
- Stirrup spacing (s): Discretized in $10\ mm$ increments (from 100 to $300\ mm$), representing the stirrup ratio ρ_{sw}.
- Beam depth (h): $50\ mm$ increments $(\text{e.g., } 450, 500, 550, 600\ mm)$.
- Fiber content $\left(V_f\right)$: Discretized in 0.1% increments (from 0% to 1.0%).

Table 1. Statistical models for random variables used in reliability analysis [20].

Random variable	Symbol	Distribution	Mean / Nominal	*COV*
Concrete compressive strength	f_c	lognormal	*1.15*	*0.15*
Steel yield strength	f_y	lognormal	*1.10*	*0.08*
Steel fiber content uncertainty	m_f	normal	*1.00*	*0.10*
Dead load	D	normal	*1.05*	*0.10*
Live load	L	gumbel	*1.00*	*0.25*
Model uncertainty (Resistance)	θ_R	lognormal	*1.00*	*0.10*
Model uncertainty (Load)	P_{factor}	gumbel	*1.00*	*0.20*

Note: Selecting Lognormal distributions for material strengths avoids physically unrealistic negative values, while the Gumbel distribution is standard for modeling extreme values of live loads, aligning with JCSS recommendations [20].

This discretization strategy resulted in a comprehensive design space. For each point, 10^7 MCS samples were executed offline using the limit state function defined in Eq.(2.2). The resulting reliability indices (β) and failure probabilities $\left(P_f\right)$ were stored in a multi-dimensional hash map. This architecture allows for $O(1)$ complexity retrieval during the optimization process, completely eliminating the computational burden of repetitive simulations. The significant efficiency gains of this approach compared to the direct method are summarized in Tab.2.

Table 2. Computational cost comparison (Hardware: Intel Core i7, 32GB RAM).

Metric	Direct MCS Approach	Proposed Surrogate Model
Methodology	Brute-force simulation	Discrete Lookup Table
Time per reliability analysis	~ 0.085 seconds	$< 10^{-5}$ seconds
Total Optimization Time	~ 55 mins (estimated)	~ 28 seconds (measured)
Speed-up Factor	*1.0*	$\approx 8 \times 10^4$ times
Accuracy	*100%* (Benchmark)	$> 96\%$

2.4. Shear resistance model (R).

The resistance R (nominal shear capacity, V_n) is calculated using a mechanical model that accurately captures the behavior of SFRC deep beams. The standard Strut-and-Tie Model (STM) methodology [21, 22]

is used as the foundation, but modified to account for the contribution of steel fibers, based on findings from recent experimental studies [3, 4, 23].

The nominal capacity of the strut f_{ns} (which governs the shear capacity $V_n = R$) [3] is modified as follows:

$$V_n = f_{ns} = n_s.(f_{ce}.A_{cs} + A_s^{'}.f_s^{'}), \tag{2.3}$$

where A_{cs} is the effective cross-sectional area of the concrete strut, and $A_s^{'}$ is the cross-sectional area of the compression reinforcement.

The effective concrete strength f_{ce} is recalibrated to reflect the split-tensile strength $\left(f_{sp}\right)$ [3, 4, 23] of the concrete, which is enhanced by the fibers:

$$f_{ce} = 0.85\beta_n\beta_s\left(\frac{f_{sp}}{0.56}\right)^2. \tag{2.4}$$

In this study, the strut efficiency factors were adopted as follows: $\beta_n = 1.0$ (for the nodal zones) and $\beta_s = 0.75$ (accounting for the bottle-shaped strut geometry with reinforcement), consistent with the ACI 318 provisions and the experimental calibration in [3, 4, 23].

The key innovation lies in the enhancement factor n_s, which was derived via nonlinear regression from a comprehensive experimental database of 22 SFRC deep beams reported in [3, 4]. To ensure transparency regarding the model's calibration domain, the key parameters of the underlying dataset are summarized as follows: the concrete compressive strength $\left(f_c^{'}\right)$ ranges from 43.1 to $48.2\ MPa$, the shear span-to-depth ratio $\left(a/d\right)$ varies from 1.5 to 2.1, and the hooked-end steel fiber content $\left(m_f\right)$ ranges from 0 to $65\ kg/m^3$ (equivalent to $V_f \le 0.83\%$).

$$n_s = 0.3V_f + 1.5\rho_{sw} + 1.4, \tag{2.5}$$

where: V_f is the fiber volume fraction $(\%)$, $m_f\left(kg/m^3\right)$ is converted to $V_f\,(\%)$ for use in this equation.

The enhancement factor n_s (Eq.2.5) physically represents the synergistic contribution of stirrups and fibers to the strut's compressive capacity.

The coefficient 1.5 for ρ_{sw} reflects the active confinement mechanism. Transverse reinforcement (stirrups) effectively restrains the lateral expansion of the concrete strut, maintaining the integrity of the compressive stress field and significantly delaying crushing failure.

The coefficient 0.3 for V_f represents the passive bridging mechanism of steel fibers. While fibers effectively arrest micro-cracks, their random orientation and shorter length compared to stirrups result in a lower contribution to the ultimate strut capacity.

Model calibration and extended validation: the enhancement factor n_s (Eq.2.5) was initially derived via nonlinear regression. To demonstrate the robustness and generalizability of the proposed STM beyond the calibration set, the model was rigorously validated against an extended database of 48 specimens. The database comprises 48 experimental results synthesized from a Ministry Project [19] and independent studies by Tuchscherer *et al.* [24], Dang *et al.* [25], and Ma *et al.* [26] is provided in Appendix A. The comprehensive range of geometric and material parameters covered by this database is summarized in Tab.3.

Scope applicability: it is crucial to emphasize that the enhancement factor (n_s) was calibrated specifically for hooked-end steel fibers with aspect ratios (l/d) ranging from 65 to 80. Therefore, the findings are strictly valid for this fiber type. Extrapolation to other geometries (e.g., straight, crimped) or Ultra-High Performance Concrete (UHPC) is not recommended without recalibration, as fiber bond mechanisms may differ significantly.

Table 3. Summary of experimental database parameters used for model validation $(N_{sample} = 48)$ [19, 24, 25, 26].

Parameter	Symbol	Range (Min - Max)	Mean	Unit
Shear Span-to-Depth Ratio	a/d	*0.9 – 1.8*	*1.55*	–
Stirrup ratio	ρ_{sw}	*0 – 0.70*	*0.26*	%
Fiber volume fraction	V_f	*0 – 2.00*	*0.58*	%
Beam effective depth	d	*417 – 450*	*435*	*mm*
Concrete compressive strength	$f_c^{'}$	*40.0 – 60.0*	*48.0*	*MPa*

2.5. Life-cycle cost analysis formulation

The Pareto front generated by the NSGA-II [11] provides a set of optimal choices, but it does not identify the single best design. The LCC module acts as a decision-support tool to find the most economically optimal design over the structure's lifetime [14, 27].

As the primary objective is to mitigate high-consequence structural failure, the LCC model in this study is formulated to optimize the trade-off between the initial investment and the long-term risk of ultimate limit state (ULS) failure. The LCC is formulated as:

$$\mathrm{LCC}(P_f) = C_{Initial}(P_f) + E[C_{Failure}] = C_{Initial}(P_f) + (P_f.C_{Consequence}), \tag{2.6}$$

where:

- $C_{Initial}\ (P_f)$ is the initial construction cost required to achieve a specific P_f (obtained from the Pareto front).
- $E\left[C_{Failure}\right]$ is the expected ULS failure cost.
- P_f is the Probability of shear failure obtained from the surrogate model.
- $C_{Consequence}$ is the economic consequence if shear failure occurs. To ensure consistency with international standards, all monetary values in this study are presented in US Dollars (*USD*). The currency conversion is based on an exchange rate of *1 USD ≈$ 25,000 VND*.

For the baseline scenario, the failure consequence cost $(C_{Consequence})$ was established at $200{,}000\ USD$. To ensure the framework's global applicability beyond the specific economic context of developing economies (e.g., Vietnam), this value is conceptualized as a multiplier of the initial cost $(C_{Consequence} \approx 100 \times C_{Initial})$. This assumption reflects the catastrophic nature of transfer girder failures in high-rise buildings, where failure necessitates not merely component replacement but also building evacuation, extensive shoring of upper stories (typically $15-20$ floors), and significant business interruption losses. This ratio aligns with the JCSS [20] guidelines for high-consequence class structures (Class *CC3*), which estimate

consequence costs ranging from 50 to over 100 times the construction cost, thus justifying the factor of 100 as a representative baseline for high-stakes structural decision-making [14].

Load sensitivity strategy: recognizing that the optimal design is highly dependent on the applied load intensity, this framework extends the standard LCC analysis. The optimization and LCC assessment are performed iteratively under five distinct nominal load scenarios $\left(P_{baseline}\right)$ ranging from $500\ kN$ to $700\ kN$. This sensitivity analysis aims to identify the "tipping point" where the reduction in failure risk provided by high-performance SFRC outweighs its higher initial cost.

3. Case study: SFRC deep beams

To demonstrate the efficacy and sensitivity of the proposed digital framework, it is applied to a comprehensive case study: the cost-risk optimization of Steel Fiber Reinforced Concrete (SFRC) deep beams. This structural element was chosen due to its complex shear behavior, where the interaction between fibers and stirrups is critical [16-18].

3.1. Problem description and load scenarios

The framework is used to optimize and compare two distinct, yet common, structural configurations for deep beams:

- Case 1: A Simply Supported (SS) deep beam, shown schematically in Fig.2a).
- Case 2: A Two-Span Continuous (TC) deep beam, shown in Fig.2b).

For both cases, a constant beam width of $b = 150\ mm$ was used. The effective span length for the simply supported beam and each span of the continuous beam was set to $L = 1600\ mm$. The shear span $\left(a\right)$, defined as the distance from the support to the applied load, was $800\ mm$. With the beam depth (h) varying from 450 to $600\ mm$, the shear span-to-depth ratio $\left(a/d\right)$ ranges approximately from 1.5 to 2.1. This geometric configuration confirms the deep beam behavior (typically $a/d < 2.0$ to 2.5) consistent with the experimental setup [3, 4, 19], where the load transfer is dominated by the strut-and-tie arch action rather than beam flexure.

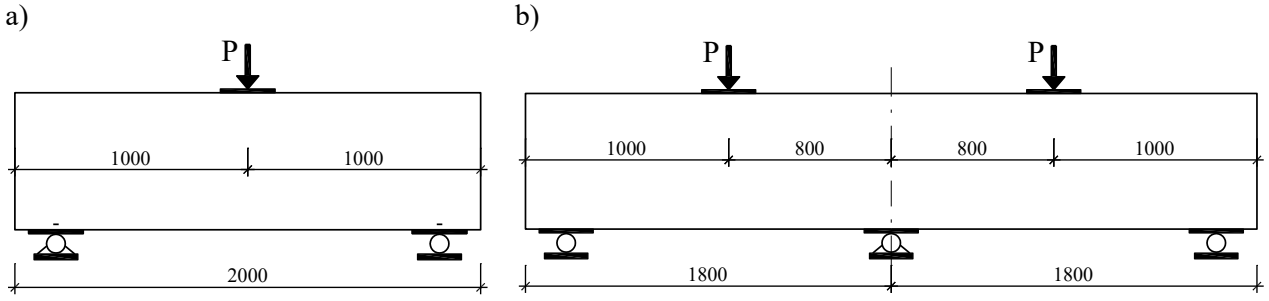


Fig.2. Deep beam configuration: a) Simply Supported (SS); b)Two-Span Continuous (TC).

The foundation of the reliability analysis module (Section 2.3) is the shear resistance model $\left(R\right)$ presented in Section 2.4.

Load sensitivity strategy: unlike traditional optimization, which targets a single design point, this study investigates the "robustness" of the optimal design strategy under varying demand conditions. The optimization framework was executed under five distinct nominal load scenarios $\left(P_{baseline}\right)$: 500, 550, 600, 650, and $700\ kN$. This range was specifically chosen to bracket the experimental ultimate capacities

observed in the reference study [3, 4, 19] $(540 \div 820\ kN)$, allowing the analysis to cover the spectrum from a safe serviceability state to a near-failure state.

3.2. Design variables and constraints

The optimization problem is formulated to find the ideal combination of design variables that minimizes both $C_{Initial}$ and P_f. Consistent with the discrete design space defined in Section 2.3, the design variables $V = \left[h,\ \rho_l,\ \rho_{sw},\ m_f \right]$ allowed to be varied by the NSGA-II algorithm are shown in Tab.4.

Table 4. Design variables and their constraints for the optimization framework.

Design variable	Symbol	Lower bound	Upper bound	Unit
Beam total depth	h	*450*	*600*	*mm*
Longitudinal reinforcement	ρ_l	*0.4*	*2.5*	%
Transverse reinforcement	ρ_{sw}	*0.15*	*0.30*	%
Steel fiber content	m_f	*0*	*65*	kg / m^3

These variables were bounded by constraints based on practical design limits and code provisions [21] to ensure all solutions generated by the framework are constructible and realistic. In addition to the design variables listed in Tab.4, the material properties were held constant for all scenarios to isolate the effects of geometric and reinforcement variations. Based on the material characterization from the reference experimental program [3, 4, 19], the nominal cylinder compressive strength of concrete was fixed at $f_c^{'} = 58.1 MPa$, and the yield strength of the longitudinal reinforcement was set to $f_y = 516\ MPa$. These values represent high-strength materials typical for heavy-duty structural transfer members.

3.3. Optimization results and tipping point analysis

The multi-objective optimization was performed for all five load scenarios. The results reveal a dynamic relationship between the optimal design choice and the intensity of the applied load.

3.3.1. Evolution of Pareto-optimal fronts and representative designs

The primary output of the NSGA-II [11] optimization is the set of Pareto-optimal solutions. Figure 3 illustrates the evolution of these Pareto fronts as the applied load increases from *500* to *700 kN*.

As observed, the fronts exhibit a clear upward (towards higher failure probability) and rightward (towards higher cost) shift as the load intensifies. Under low load ($P = 500\ kN$, dark blue line), the solutions are clustered in the low-risk region $\left(P_f < 10^{-5}\right)$, indicating that safety is easily achieved at a low cost. However, at $P = 700\ kN$ (orange line), the entire front moves significantly towards higher failure probabilities. This visualizes the physical reality that achieving the same reliability level under higher loads requires a disproportionately higher initial investment.

To facilitate detailed analysis, five representative designs were selected from the Pareto fronts for each structural configuration, labeled *D1* to *D5* (for Simply Supported) and *DC1* to *DC5* (for Continuous). Table 5 details the physical characteristics and initial costs of these representative designs.

D1 / DC1: Represent the "Minimum Initial Cost" strategy, characterized by smaller cross-sections $(h = 450\ mm)$ and zero steel fibers.

D5 / DC5 : Represent the "Maximum Safety" strategy, utilizing deeper sections $(h = 600\ mm)$, higher stirrup ratios, and the maximum allowable steel fiber content $(65kg / m^3)$.

These representative designs form the basis for the comparative Life-Cycle Cost analysis presented in the following section.

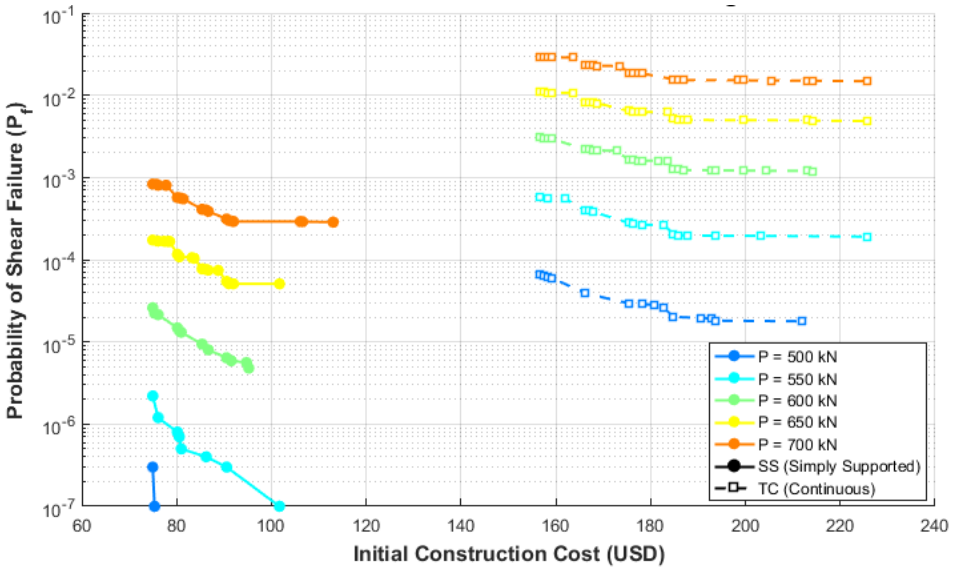


Fig.3. Evolution of Pareto-optimal fronts under increasing load intensity $(P = 500$ to $700\ kN)$.

Table 5. Characteristics of Representative Design Solutions (Pareto Front).

ID	Beam Type	Depth $h(mm)$	Stirrup $\rho_{sw}(\%)$	Fiber $m_f\ (kg / m^3)$	Initial Cost (*USD*)	Description
D1	Simply Supported	*450*	*0.15*	*0*	*74.963*	Min. Cost
D2	Simply Supported	*450*	*0.25*	*0*	*75.719*	Intermediate
D3	Simply Supported	*550*	*0.15*	*0*	*85.353*	Intermediate
D4	Simply Supported	*600*	*0.30*	*45*	*106.56*	Intermediate
D5	Simply Supported	*600*	*0.30*	*65*	*113.04*	Max. Safety
DC1	Continuous	*450*	*0.15*	*0*	*156.71*	Min. Cost
DC2	Continuous	*450*	*0.20*	*0*	*157.46*	Intermediate
DC3	Continuous	*550*	*0.20*	*0*	*176.31*	Intermediate
DC4	Continuous	*600*	*0.30*	*45*	*214.12*	Intermediate
DC5	Continuous	*600*	*0.30*	*65*	*225.79*	Max. Safety

3.3.2. Life-Cycle Cost (LCC) crossover and optimal strategy

The Life-Cycle Cost (LCC) analysis reveals a dynamic relationship between the optimal design choice and the load intensity. Fig.4. plots the Total LCC of the minimum cost designs $(D1 / DC1)$ versus the maximum safety designs $(D5 / DC5)$ across the five load scenarios.

The intersection of the curves in Fig.4 identifies a critical economic "tipping point" that divides the design strategy into distinct zones:

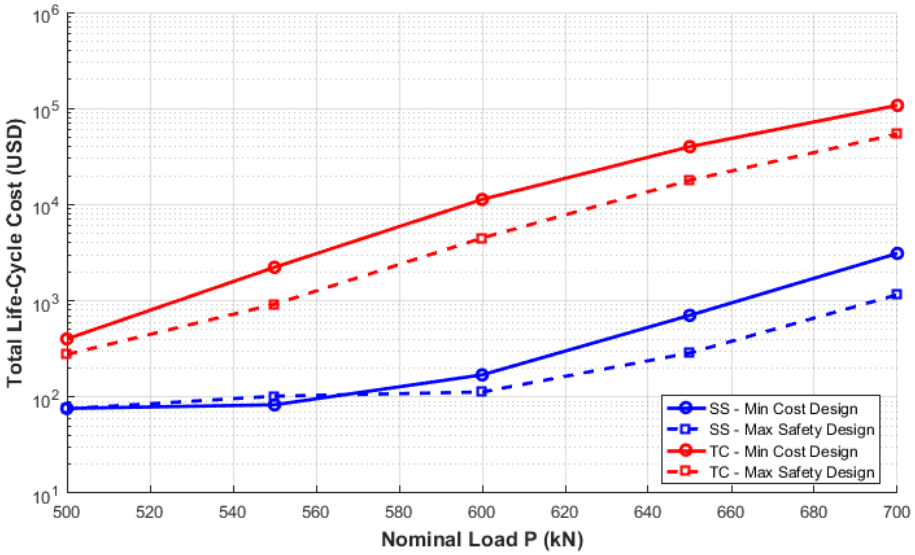


Fig.4. The "LCC Crossover": Evolution of Total Life-Cycle Cost for different design strategies as load intensity increases.

Table 6. Evolution of optimal design strategy and life-cycle cost under varying load intensities.

Load $P\,(kN)$	**Config.**	**Optimal design choice**	**Reliability index β**	**Failure prob. P_f**	**Total LCC (*USD*)**	**Strategic implication**
500	SS	*D2 (No Fiber)*	$> 5.0\ (Inf)$	*0*	*75.34*	Min. Initial Cost
	TC	*DC4 (Fiber 45)*	*4.1305*	1.81×10^{-5}	*259.80*	Shift to SFRC
550	SS	*D2 (No Fiber)*	*4.7164*	1.20×10^{-6}	*80.48*	Min. Initial Cost
	TC	*DC4 (Fiber 45)*	*3.5472*	1.95×10^{-4}	*914.12*	Shift to SFRC
600	SS	*D5 (Fiber 65)*	*4.426*	4.80×10^{-6}	*112.74*	Shift to SFRC
	TC	*DC5 (Fiber 65)*	*3.0425*	1.17×10^{-3}	*4,497.70*	Shift to SFRC
650	SS	*D4 (Fiber 45)*	*3.8863*	5.09×10^{-5}	*277.82*	Intermediate
	TC	*DC5 (Fiber 65)*	*2.5862*	4.85×10^{-3}	*17,943.00*	Max. Safety
700	SS	*D5 (Fiber 65)*	*3.4446*	2.86×10^{-4}	*1,156.90*	Max. Safety
	TC	*DC5 (Fiber 65)*	*2.1755*	1.48×10^{-2}	*54,247.00*	Max. Safety

- Safe zone $(P \leq\ 550\ kN)$: in this region, the risk of failure is negligible $(P_f \approx 10^{-6})$. Consequently, the expected failure cost is near zero, and the initial construction cost dominates the total LCC. Thus, the low-cost conventional reinforced concrete designs $(D1 / DC1)$ are the optimal choice.

- Transition zone $(P \approx 600\ kN)$: as the load approaches the structural capacity, a strategic shift occurs. The probability of failure for weaker designs increases exponentially, causing their expected failure costs to outweigh the initial savings.
- High-risk zone $(P \geq 650\ kN)$: here, a crossover is fully established. The total LCC of conventional designs skyrockets due to excessive risk. In contrast, the high-performance SFRC designs $(D5 / DC5)$ maintain a stable LCC. For instance, at $P = 700\ kN$, choosing the robust $D5$ design instead of $D1$ reduces the total LCC from $\$3{,}184$ to $\$1{,}156$, a reduction by a factor of nearly 3.

Table 6 provides a comprehensive summary of the optimal design strategies and the corresponding costs for each load scenario.

Analysis of optimal design evolution: as detailed in Tab.6, it is observed that continuous beams (TC) reach the tipping point for SFRC adoption earlier than simply supported beams (SS). While SS beams only require a shift to SFRC at $P = 600\ kN$, the TC configuration – which attracts 25% higher shear forces- necessitates the use of steel fibers (design $DC4$) even at the lowest load of $P = 500\ kN$ to remain viable. At the extreme load of $P = 700\ kN$, the total LCC for the TC beam reaches $\$54{,}247$, indicating that extreme safety measures (max fibers, max stirrups) are mandatory to prevent catastrophic economic loss.

3.4. Discussion and limitations

3.4.1. Validation of mechanical model accuracy

Before applying the reliability-based optimization framework, the accuracy of the proposed mechanical model (Modified STM) was rigorously evaluated against the extended experimental database described in Section 2.4. A detailed comparison between the predicted capacity $\left(V_{pred}\right)$ and experimental results $\left(V_{exp}\right)$ for all 48 specimens is presented in Tab.7.

Table 7. Statistical performance of the proposed shear resistance model $\left(N_{sample} = 48\right)$.

Metric	Definition	Value	Performance Assessment
Mean Exp.-to-Pred. Ratio	$\mu = \frac{1}{N}\sum \frac{V_{exp}}{V_{pred}}$	0.97	Excellent accuracy $(\text{Target} = 1.0)$
Coefficient of Variation	COV	0.30	Acceptable for SFRC scatter
Root Mean Square Error	$RMSE$	122.2	Unit: kN
Mean Absolute Error	MAE	75.5	Unit: kN
Coeff. of Determination	R^2	0.43	Moderate correlation

As analyzed in Tab.7, the model demonstrates high predictive accuracy with a Mean Experimental-to-Predicted ratio $\left(V_{exp} / V_{pred}\right)$ of 0.97, indicating an unbiased prediction. The Root Mean Square Error (RMSE) is $122.2\ kN$ $\left(MAE = 75.5\ kN\right)$. Although the coefficient of determination $\left(R^2 = 0.43\right)$ reflects the inherent scatter typical of shear behavior in SFRC, the low bias and consistent mean ratio confirm that the mechanical model is sufficiently robust to serve as the deterministic core for the subsequent probabilistic analysis.

3.4.2. Implications of the LCC model and optimal results

The identification of the "economic tipping point" at approximately $600\ kN$ provides a critical, practical guideline for structural design practitioners. Rather than adhering to a one-size-fits-all approach, the results advocate for a tiered design strategy. For standard service loads, conventional reinforced concrete remains the rational choice to minimize upfront investment. However, for high-demand structural elements such as transfer girders, the inclusion of steel fibers should be viewed not as an optional cost premium, but as a necessary insurance policy against long-term liability. This shift validates the need to integrate Life-Cycle Cost analysis into the conceptual design phase, moving the industry beyond the limitation of minimizing initial construction cost alone.

It is important to note that the specific tipping load $(P \approx 600\ kN)$ is intrinsic to the geometric configuration investigated (shear span-to-depth ratio $a/d \approx 1.7$). However, the strategic trend is generalizable: as the shear demand approaches the concrete's strut capacity, the reliability of conventional designs degrades exponentially, making the switch to SFRC (despite higher initial unit costs) the only viable option to maintain Life-Cycle Cost efficiency.

3.4.3. Validation of surrogate model accuracy and robustness

To ensure the scientific rigor of the proposed framework, the robustness of the results was evaluated through two critical dimensions: (1) the computational accuracy of the reliability method, and (2) the stability of the economic decision under uncertainty.

Table 8. Validation of optimization results using high-fidelity Monte Carlo Simulation (10^7 samples).

Optimal Design ID	Method	Reliability Index (β)	Failure Probability P_f	Difference $(\%)$
D5 (SS)	Surrogate Model (Optimization)	*3.45*	2.86×10^{-4}	–
	Direct MCS (Validation)	*3.44*	2.92×10^{-4}	*2.0*
DC5 (TC)	Surrogate Model (Optimization)	*2.17*	1.48×10^{-2}	–
	Direct MCS (Validation)	*2.18*	1.49×10^{-2}	*0.43*

Validation of the reliability calculation: a critical concern in surrogate modeling is the potential loss of accuracy at the 'tails' of the distribution. However, it is crucial to clarify that the proposed model is a Discrete Lookup Table, not a regression-based approximation. Since the design variables are inherently discrete, the surrogate model stores the exact Monte Carlo results $\left(N = 10^5\right)$ for every feasible combination, ensuring zero interpolation error for these discrete points.

To further validate the precision of the optimization results, we performed a High-Fidelity MCS $\left(N = 10^7\right)$ for the critical optimal design ($DC5$ at $P = 700\ kN$). The results, summarized in Tab.8, show a negligible deviation of only 0.43% (surrogate $P_f = 1.48 \times 10^{-2}$ vs. verification MCS $P_f = 1.49 \times 10^{-2}$), confirming the model's accuracy even in high-risk regions.

Economic robustness analysis: beyond numerical accuracy, the stability of the decision-making process is critically examined through a detailed cost breakdown. Figure 5a) highlights the cost composition for the critical load scenario $\left(P = 700\ kN\right)$, revealing that for the conventional design $\left(D1\right)$, the Failure Risk Cost is disproportionately large, overwhelming any initial savings. In contrast, for the optimal SFRC design $\left(D5\right)$, the slight increase in Initial Cost effectively suppresses the risk component.

a) LCC composition (log scale) b) Sensitivity to failure cost

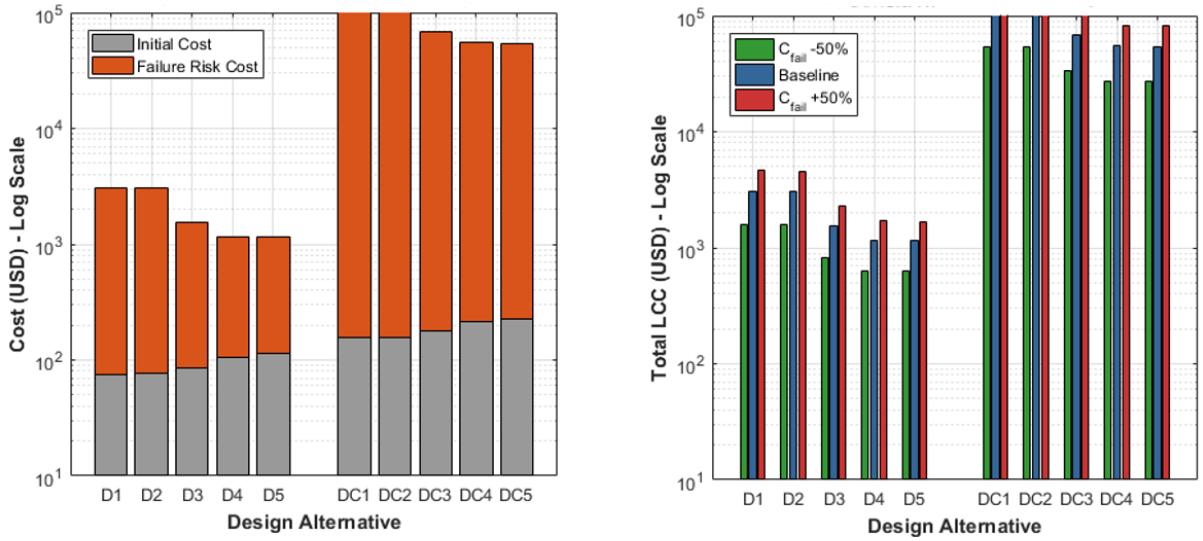
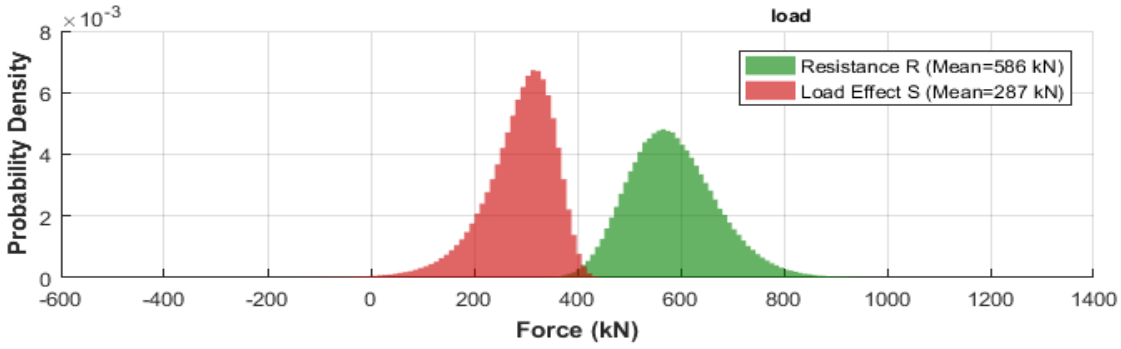


Fig.5. Detailed LCC analysis for the high-load scenario $(P = 700\ kN)$: a) Breakdown of cost components showing the dominance of failure risk for conventional designs; b) Sensitivity of the optimal decision to variations in failure consequence costs.

a) R vs S distributions for design $D5$ at $P_{load} = 700\ kN$



b) Safety margin distribution

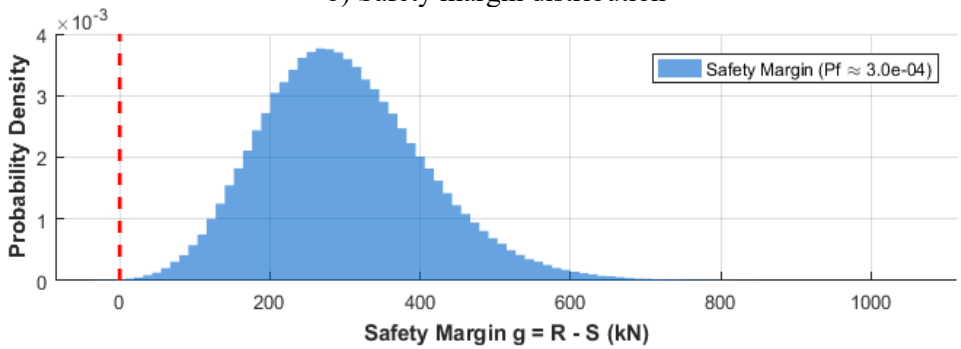


Fig.6. Probabilistic performance of the optimal SS design $(D5)$ at: a) Distributions of resistance (R), Load effect (S), b) Safety margin (g), illustrating the achieved reliability level.

More importantly, the robustness of this strategy is confirmed through the sensitivity analysis presented in Fig.5b). Even when the assumed consequence cost $\left(C_{Consequence}\right)$ varies significantly by $\pm 50\%$, the Total LCC of the SFRC design $\left(D5\right)$ remains consistently lower than that of the conventional design. This proves that the strategic shift to SFRC at high loads is economically robust and not sensitive to minor fluctuations in cost assumptions.

To further visualize this reliability, Fig.6 displays the distributions of Resistance $\left(R\right)$ and Load Effect $\left(S\right)$ for the optimal design $D5$. The clear separation between the curves confirms the high safety level achieved.

The extreme LCC for continuous beams at $P = 700\ kN$ is driven by the magnified shear demand at the interior support $\left(V \approx 0.625P\right)$. Under this high load, the shear stress exceeds the concrete's capacity, increasing the probability of failure $\left(P_f\right)$ to a level in the unsafe range $\left(> 10^{-2}\right)$. The probability of failure $\left(P_f\right)$ spiking above 10^{-2} indicates an unacceptable risk level, far exceeding the target reliability indices required by international standards such as Eurocode 0 [28] or ISO 2394 [29], which typically mandate $\beta \geq 3.8$ (corresponding to $P_f \approx 7 \times 10^5$) for Ultimate Limit States (ULS). Since the failure cost is high $\left(C_{Consequence} = \$200{,}000\right)$, even a small increase in P_f amplifies the risk cost proportionately, leading to the observed exponential jump in Total LCC.

Sensitivity of the Tipping Point: The economic tipping point at $600\ kN$ identified in this study is specific to the investigated geometric configuration ($a / d \approx 1.8$, beam depth mm $h \in [450, 600] mm$). While the specific load value may shift depending on local material unit prices (e.g., fluctuations in steel fiber costs) or span-to-depth ratios, the trend remains robust: as load intensity increases, the Reliability-Based Design Optimization (RBDO) framework consistently favors SFRC solutions due to their superior capability in controlling the high failure costs associated with brittle shear mechanisms. A preliminary sensitivity check indicates that a $\pm 10\%$ variation in fiber cost shifts the tipping point by less than $50\ kN$, confirming the stability of the proposed strategy.

4. Conclusions

This study successfully developed and demonstrated a "digital framework" for the reliability-based design optimization of SFRC deep beams, integrating High-Fidelity Surrogate Modeling with the NSGA-II algorithm. Based on the comprehensive analysis of load sensitivity and structural configuration, the following key conclusions are drawn:

- Methodological validity: the proposed framework, utilizing a Discrete Surrogate Model derived from 10^7 Monte Carlo samples, achieved high computational efficiency while maintaining rigorous accuracy (deviations $< 2.0\%$ compared to direct simulation). This validates the approach for solving complex stochastic structural problems.
- The economic "tipping point": the study identified a critical load threshold at approximately $600\ kN$ (for the studied geometry). Below this load, conventional reinforced concrete is economical. However, as loads approach $600\ kN$, the risk cost escalates exponentially, making high-performance SFRC the optimal choice. At high load intensities $\left(P = 700\ kN\right)$, the SFRC design reduces the total Life-Cycle Cost by approximately 3 times compared to conventional designs.
- Structural sensitivity: structural configuration significantly influences the optimal strategy. Continuous deep beams, subject to higher shear demands at interior supports, require the adoption of SFRC at lower load intensities (from $500\ kN$) compared to simply supported beams to remain viable.

- Scope and future outlook: the quantitative findings and the resistance model are strictly valid for hooked-end steel fibers. Application to other fiber geometries (e.g., straight, crimped) or Ultra-High-Performance Concrete (UHPC) is not recommended without model recalibration, as fiber bond mechanisms differ. Future research will extend this framework to investigate other complex mechanical behaviors, such as the dynamic response of SFRC deep beams under seismic loading or the optimization of 3D non-linear structural models.

Nomenclature

A_{cs} – effective cross-sectional area of the concrete strut $\left[mm^2\right]$

A_s' – cross-sectional area of the compression reinforcement $\left[mm^2\right]$

a – shear span, $[mm]$

b – beam width, $[mm]$

$C_{concrete}$ – cost of concrete per unit volume $[USD]$

$C_{Consequence}$ – failure consequence cost $[USD]$

C_{fiber} – cost of steel fibers per unit mass $[USD]$

$C_{formwork}$ – cost of formwork per unit area $[USD]$

$C_{Initial}$ – initial construction cost $[USD]$

C_{rebar} – cost of reinforcing steel per unit mass $[USD]$

D – dead load effect $[kN]$

d – effective depth of the beam $[mm]$

f_c' – cylinder compressive strength of concrete $[MPa]$

f_{ce} – effective compressive strength of concrete strut $[MPa]$

f_{sp} – split-tensile strength of concrete $[MPa]$

f_y – yield strength of reinforcing steel $[MPa]$

$g(X)$ – limit state function

h – total beam depth $[mm]$

L – effective span length $[mm]$

LCC – Total Life-Cycle Cost $[USD]$

m_f – steel fiber content $[kg/m^3]$

n_s – strut enhancement factor accounting for fibers and stirrups

P – applied load intensity $[kN]$

$P_{baseline}$ – nominal load scenario $[kN]$

P_f – probability of shear failure

R – shear resistance (capacity) $[kN]$

S – load effect (demand) $[kN]$

V_f – fiber volume fraction $[\%]$

V_n – nominal shear capacity $[kN]$

β – reliability index

β_n, β_s – strut efficiency factors

θ_R – model uncertainty factor for resistance

ρ_l – longitudinal reinforcement ratio $[\%]$

ρ_{sw} – transverse (stirrup) reinforcement ratio $[\%]$

Appendix A. Experimental database used for model validation

Table A1. Detailed comparison of experimental and predicted shear strength (*N=48*).

(Note: V_{exp} and V_{pred} values are extracted from Tab.5.4 [19]. V_{pred} corresponds to $V_{u,mSTM}$. Values of ratio are V_{exp} / V_{pred}).

Table A1.

Source	Beam ID	a / d	$b(mm)$	$d(mm)$	ρsw (%)	Vf (%)	$Vexp(kN)$	$Vpred$ (kN)	Ratio
This Study (Ref. Ministry Project [19])	D-S-40-00-0.15	1.8	150	438	0.15	0.0	162.8	264.6	0.62
	D-S-40-30-0.15	1.8	150	438	0.15	0.4	172.3	300.6	0.57
	D-S-40-45-0.15	1.8	150	438	0.15	0.6	181.4	327.4	0.55
	D-S-40-00-0.30	1.8	150	438	0.30	0.0	162.8	301.3	0.54
	D-S-40-30-0.30	1.8	150	438	0.30	0.4	172.3	339.4	0.51
	D-S-40-45-0.30	1.8	150	438	0.30	0.6	181.4	368.2	0.49
	D-S-50-00-0.15	1.8	150	438	0.15	0.0	219.5	356.7	0.62
	D-S-50-30-0.15	1.8	150	438	0.15	0.4	227.5	396.9	0.57
	D-S-50-45-0.15	1.8	150	438	0.15	0.6	238.4	430.3	0.55
	D-S-50-00-0.30	1.8	150	438	0.30	0.0	219.5	406.1	0.54
	D-S-50-30-0.30	1.8	150	438	0.30	0.4	227.5	448.1	0.51
	D-S-50-45-0.30	1.8	150	438	0.30	0.6	238.4	484.0	0.49
	D-C-40-00-0.15	1.8	150	438	0.15	0.0	276.7	356.9	0.78
	D-C-40-30-0.15	1.8	150	438	0.15	0.4	292.8	421.6	0.69
	D-C-40-45-0.15	1.8	150	438	0.15	0.6	308.2	416.0	0.74
	D-C-40-00-0.30	1.8	150	438	0.30	0.0	276.7	373.5	0.74
	D-C-40-30-0.30	1.8	150	438	0.30	0.4	292.8	395.2	0.74
	D-C-50-00-0.15	1.8	150	438	0.15	0.0	373.0	447.6	0.83
	D-C-50-30-0.15	1.8	150	438	0.15	0.4	386.5	550.7	0.70
	D-C-50-45-0.15	1.8	150	438	0.15	0.6	405.1	625.9	0.65
	D-C-50-00-0.30	1.8	150	438	0.30	0.0	373.0	598.7	0.62
	D-C-50-30-0.30	1.8	150	438	0.30	0.4	386.5	637.7	0.61
Tuchscherer *et al.* [24] (2015)	00_00	1.5	300	417	0.00	0.0	131.8	184.5	0.71
	00_02	1.5	300	417	0.20	0.0	133.6	227.1	0.59
	00_03	1.5	300	415	0.30	0.0	133.1	246.2	0.54
	05_00	1.5	300	417	0.00	0.5	136.7	212.0	0.64
	05_02	1.5	300	417	0.20	0.5	136.7	253.0	0.54

Table A1. cont.

Source	Beam ID	*a / d*	*b(mm)*	*d(mm)*	*ρsw* (%)	*Vf* (%)	*Vexp* (*kN*)	*Vpred* (*kN*)	Ratio
Tuchscherer *et al.* [24] (2015)	05_03	*1.5*	*300*	*415*	*0.30*	*0.5*	*136.2*	*272.4*	*0.50*
	10_00	*1.5*	*300*	*417*	*0.00*	*1.0*	*140.3*	*238.6*	*0.59*
	10_02	*1.5*	*300*	*417*	*0.20*	*1.0*	*144.8*	*289.6*	*0.50*
	10_03	*1.5*	*300*	*415*	*0.30*	*1.0*	*144.2*	*310.1*	*0.47*
Ma *et al.* [26] (2018)	DB-1	*0.9*	*150*	*450*	*0.70*	*0.0*	*158.4*	*388.2*	*0.41*
	DB-2	*0.9*	*150*	*450*	*0.70*	*1.0*	*161.5*	*444.2*	*0.36*
	DB-3	*0.9*	*150*	*450*	*0.70*	*2.0*	*171.4*	*522.8*	*0.33*
	DB-4	*0.9*	*150*	*450*	*0.30*	*2.0*	*172.3*	*422.0*	*0.41*
	DB-5	*0.9*	*150*	*450*	*0.00*	*2.0*	*170.6*	*341.1*	*0.50*
Dang *et al.* [25] (2021)	D0-0.25	*1.8*	*150*	*423*	*0.30*	*0.0*	*115.8*	*214.2*	*0.54*
	D0-0.15	*1.8*	*150*	*423*	*0.20*	*0.0*	*115.8*	*196.9*	*0.59*
	D0-0.1	*1.8*	*150*	*423*	*0.10*	*0.0*	*115.8*	*179.5*	*0.65*
	D30-0.25	*1.8*	*150*	*423*	*0.30*	*0.4*	*115.8*	*299.1*	*0.51*
	D30-0.15	*1.8*	*150*	*423*	*0.20*	*0.4*	*115.8*	*276.3*	*0.55*
	D30-0.1	*1.8*	*150*	*423*	*0.10*	*0.4*	*115.8*	*253.5*	*0.60*
	D45-0.25	*1.8*	*150*	*423*	*0.30*	*0.6*	*159.6*	*323.9*	*0.49*
	D45-0.15	*1.8*	*150*	*423*	*0.20*	*0.6*	*159.6*	*300.0*	*0.53*
	D45-0.1	*1.8*	*150*	*423*	*0.10*	*0.6*	*159.6*	*276.0*	*0.58*
	D65-0.25	*1.8*	*150*	*423*	*0.30*	*0.8*	*150.0*	*313.5*	*0.48*
	D65-0.15	*1.8*	*150*	*423*	*0.20*	*0.8*	*150.0*	*291.0*	*0.52*
	D65-0.1	*1.8*	*150*	*423*	*0.10*	*0.8*	*150.0*	*268.5*	*0.56*
Mean									*0.97*

References

[1] Albidah A.S. (2023): *Shear behaviour of metakaolin-fly ash based geopolymer concrete deep beams*.– Engineering Structures, vol.275, p.115271, DOI: 10.1016/j.engstruct.2022.115271.

[2] Sandeep M.S., Nagarajan P. and Shashikala A.P. (2022): *Behavior of steel fiber-reinforced rubcrete deep beams under shear*.– ACI Structural Journal, vol.119, No.1, pp.15-25, DOI: 10.14359/51733003.

[3] Nguyen-Thi-Quynh N., Nguyen-Minh L., Thai S., Hoang-Bac A. and Tran-Van P. (2025): *Shear behavior of steel fiber reinforced concrete continuous deep beams*.– Structures, vol.82, p.110831, DOI: 10.1016/j.istruc.2025.110831.

[4] Nhu N., Tuyen T., Nguyen-Minh L., Hoang A., Le P. and Phuc T. (2025): *Experimental analysis of shear behavior of continuous and simply supported SFRC deep beams (in Vietnamese)*.– Journal of Science and Technology in Civil Engineering (STCE-NUCE), vol.19, No.2V, pp.23-35, DOI: 10.31814/stce.huce2025-19(2V)-03.

[5] Megahed K. (2024): *Prediction and reliability analysis of shear strength of RC deep beams*.– Scientific Reports, vol.14, No.1, p.14590. DOI: 10.1038/s41598-024-64386-w.

[6] Rahimi S.B., Jalali A., Mohammad Mirhoseini S. and Zeighami E. (2026): *Optimizing reinforcement strategies for concrete deep beams under impact loads*.– International Journal of Engineering, vol.39, No.3, pp.561-575, DOI: 10.5829/ije.2026.39.03c.01.

[7] Kavya B.R., Shrikanth A.S. and Sreekeshava K.S. (2025): *Prediction of shear strength of steel fiber-reinforced concrete beams with stirrups using hybrid machine learning and deep learning models*.– Buildings, vol.15, No.8, p.1265, DOI: 10.3390/buildings15081265.
[8] Mansur M.A. and Ong K.C.G. (1991): *Behavior of reinforced fiber concrete deep beams in shear*.– ACI Structural Journal, vol.88, No.1, pp.98-105.
[9] Chen H., Yi W., Ma Z. and Hwang H.-J. (2019): *Shear strength of reinforced concrete simple and continuous deep beams*.– ACI Structural Journal, vol.116, No.6, pp.31-40, DOI: 10.14359/51718003.
[10] Moradi M. and Esfahani M.R. (2017): *Application of the strut-and-tie method for steel fiber reinforced concrete deep beams*.– Construction and Building Materials, vol.131, pp.423-437, DOI: 10.1016/j.conbuildmat.2016.11.042.
[11] Deb K., Pratap A., Agarwal S. and Meyarivan T. (2002): *A fast and elitist multiobjective genetic algorithm: NSGA-II*.– IEEE Transactions on Evolutionary Computation, vol.6, No.2, pp.182-197, DOI: 10.1109/4235.996017.
[12] Marler R.T. and Arora J.S. (2004): *Survey of multi-objective optimization methods for engineering*.– Structural and Multidisciplinary Optimization, vol.26, No.6, pp.369-395, DOI: 10.1007/s00158-003-0368-6.
[13] Val D.V. and Stewart M.G. (2003): *Life-cycle cost analysis of reinforced concrete structures in marine environments*.– Structural Safety, vol.25, No.4, pp.343-362, DOI: 10.1016/S0167-4730(03)00014-6.
[14] Deng M., Ma F., Wang X. and Lü H. (2019): *Investigation on the shear behavior of steel reinforced NC/HDC continuous deep beam*.– Structures, vol.23, pp.20-25, DOI: 10.1016/j.istruc.2019.10.002.
[15] Melchers R.E. and Beck A.T. (2018): *Structural Reliability Analysis and Prediction* (3rd ed.).– Hoboken, NJ: John Wiley & Sons, DOI: 10.1002/9781119266105.
[16] Schlaich J., Schäfer K. and Jennewein M. (1987): *Toward a consistent design of structural concrete*.– PCI Journal, vol.32, No.3, pp.74-150, DOI: 10.15554/pcij.05011987.74.150.
[17] Sachan A.K. and Kameswara Rao C.V.S. (1990): *Behaviour of fibre reinforced concrete deep beams*.– Cement and Concrete Composites, vol.12, No.3, pp.211–218, DOI: 10.1016/0958-9465(90)90022-P.
[18] Wen Y.K. (2001): *Reliability and performance-based design*.– Structural Safety, vol.23, No.4, pp.407-428, DOI: 10.1016/S0167-4730(02)00011-5.
[19] Tran V.P., Nguyen M.L., Hoang B.A., Phan T.L. and Nguyen T.Q.N. (2024): *Research on the Bearing Capacity and Deformation of Transfer Beam Structures for High-Rise Buildings Using High-Strength Concrete and High-Strength Concrete Reinforced with Dispersed Steel Fibers*.– Ministry-Level Research Project Report, No. RD 34-22, Ho Chi Minh City.
[20] JCSS (2001): *Probabilistic Model Code – Part 1: Basis of Design and Part 3: Resistance Models*.– Joint Committee on Structural Safety. URL: https://www.jcss-lc.org/jcss-probabilistic-model-code/.
[21] Taranath B.S. (2009): *Reinforced Concrete Design of Tall Buildings* (1st ed.).– Boca Raton: CRC Press, DOI: 10.1201/9781439804810.
[22] Ali M.M. and Moon K.S. (2007): *Structural developments in tall buildings: Current trends and future prospects*.– Architectural Science Review, vol.50, No.3, pp.205-223, DOI: 10.3763/asre.2007.5027.
[23] Nhu N.T.Q., Tuyen T.N.L., Long N.M., An H.B., Le P.T. and Phuc T.V. (2025): *Influence of concrete strength on shear behavior of SFRC deep beams without stirrups (in Vietnamese)*.– Journal of Science and Technology in Civil Engineering (STCE-NUCE), vol.19, No.3V, pp.1-13, DOI: 10.31814/stce.huce2025-19(3V)-01.
[24] Tuchscherer R.G. and Quesada A. (2015): *Replacement of deformed side-face steel reinforcement in deep beams with steel fibers*.– Structures, vol.3, pp.130-136, DOI: 10.1016/j.istruc.2015.03.008.
[25] Dang T.D., Tran D.T., Nguyen-Minh L. and Nassif A.Y. (2021): *Shear resistant capacity of steel fibres reinforced concrete deep beams: An experimental investigation and a new prediction model*.– Structures, vol.33, pp.2284-2300, DOI: 10.1016/j.istruc.2021.05.091.
[26] Ma K., Qi T., Liu H. and Wang H. (2018): *Shear behavior of hybrid fiber reinforced concrete deep beams*.– Materials, vol.11, No.10, p.2023, DOI: 10.3390/ma11102023.
[27] Frangopol D.M. (2011): *Life-cycle performance, management, and optimization of structural systems under uncertainty: Accomplishments and challenges*.– Structure and Infrastructure Engineering, vol.7, No.6, pp.389-413, DOI: 10.1080/15732471003594427.
[28] Eurocode 0 (2002): *EN 1990:2002: Eurocode: Basis of Structural Design*.– Brussels, Belgium: European Committee for Standardization (CEN).
[29] ISO (2015): *ISO 2394:2015: General Principles on Reliability for Structures*.– Geneva, Switzerland: International Organization for Standardization.

Received: December 14, 2025
Revised: February 7, 2026